Int. j. adv. multidisc. res. stud. 2025; 5(1):1270-1279

Received: 07-01-2025
Accepted: 17-02-2025

International Journal of Advanced Multidisciplinary Research and Studies

ISSN: 2583-049X

Thermal Performance of Hybrid Nanoparticles on Radiative Flow with Slip Boundary Condition Under the Influence of Riga Plate

[1] O Adebisi, [2] OA Ajala, [3] AA Bepo, [4] M Taiwo

[1]Department of Mathematics, Federal College of Education, Iwo, Osun State, Nigeria
[2, 3] Department of Pure and Applied Mathematics, Ladoke Akintola University of Technology, Ogbomoso, Oyo State, Nigeria
[4] Department of Physical and Chemical Sciences, Federal University of Health Sciences, Ila Orangun, Osun State, Nigeria

DOI: https://doi.org/10.62225/2583049X.2025.5.1.3793
Corresponding Author: **O Adebisi**

Abstract

The rapid development of modern nanotechnology in industries and medical area have brought about the idea of mixing more than one nanoparticle in a base fluid which is called hybrid nanofluid. Hybrid nanofluid enhances the thermophysical properties of flow better compare to nanofluid. The main object of this study is to examine the thermal performance of hybrid nanoparticles on radiative flow with slip boundary condition under the influence of Riga Plate. This lead to a mathematical flow model in terms of highly non-linear partial differential equations (PDEs). The partial differential equations and their boundary conditions were reduced to ordinary differential equations (ODEs) using a suitable similarity variable. The resulting non-linear system of equations is then solved using Chebychev Collocation Method with the aid of Mathematica 11.0 software. It is found that the heat transfer rate of the hybrid nanofluid is higher as compared to the nanofluid. The imposed magnetic field of high strength is a better tool to control the motion of hybrid nanofluids inside the boundary layer. Thermal radiations and slip parameter are observed to be beneficial for thermal enhancement for both hybrid and nanofluids.

Keywords: Hybrid Nanofliud, Slip Boundaries, Casson Fluid, Rga Plate, Radiation, Magnetohydrodynamics

1. Introduction

The utilization of magnetic fields in technological processes has garnered immense interest in recent years, owing to their potential in improving the efficiency and effectiveness of various industrial processes. In this regard, understanding the thermal mechanism in magneto-radiated systems is of significant importance in enhancing the potential applications of these systems in various technological processes. The quest for efficient heat transfer methods has led to the exploration of nanofluids, fluids containing suspended nanoparticles. This research focuses on a specific type of nanofluid; a hybrid nanofluid (hnf) composed of Fe_3O_4 (magnetite) and Ag (silver) nanoparticles suspended in ethylene glycol. Ethylene glycol, a common coolant, plays a crucial role in transporting heat within the fluid. Zeeshan *et al*. (2023) [25], demonstrated the role of nanofluid and hybrid nanofluid for enhancing thermal conductivity towards exponentially stretching curve. The research investigates the thermal mechanism within this hnf when subjected to a modified magnetic field and external radiation, the combination of a magnetic field, radiative heat source, and the unique properties of Fe_3O_4 and Ag nanoparticles is expected to influence heat generation and transfer efficiency. Understanding this mechanism will pave way for applications demanding precise temperature control, such as targeted drug delivery, microchip cooling, hybrid-powered engines, cancer therapies, geothermal power extraction, industrial cooling and thermal management in microfluidic devices. Xuan *et al*. (2022) [23] worked on guideline for selecting appropriate mixing ratio of hybrid nanofluids in thermal management system.

Magnetohydrodynamics is an investigation of electrically conductive fluid motion subjected to the external magnetic field. A magnetic field regulates the convective heat transport and fluid motion. However, it depends upon the geometry of the problem and flow conditions. Magnetic field is used in many applications like MRI, metal processing, geothermal and nuclear reactors, float glass, nuclear and power plants etc. A number of research work is done on MHD fluid flows. Awais and Salahuddin and Awais (2024) [12] described the chemical reaction and viscous dissipation effects on MHD cross flow over a paraboloid surface and computed the numerical solution. They observed that the magnetic field strongly decelerates the fluid velocity in flow regime. Ali *et al*. (2023), analyzed the physical properties of the MHD Blasius and Sakadias flows with different physical and thermal effects. They computed the numerical solution with finite element method and observed that the magnetic field, thermal condition and radiation phenomena enlarges the flow temperature significantly.

Ramzan *et al*. (2022) [20] considered the variable viscosity effects on the flow of MHD hybrid nanofluid containing dust particles over a needle with Hall current and the analytical solutions for flows of casson fluid with slip boundary conditions. The equations governing the flow of Casson fluid are non-linear in nature. Analytical solutions of the non-linear governing equations with non-linear boundary conditions are obtained for each case. The effect of the various parameters on the velocity and volume flow rate for each problem is studied and the results are presented through graphs. It is observed that, the presence of Casson number decreases the velocity and volume flow rate of the fluid. Increasing of slip parameter increases the velocity and volume flow rate in both Poiseuille and generalized Couette flows. Pattnaik *et al.* (2023) [19] considered heat transfer analysis on Engine oil-based hybrid nanofluid past an exponentially stretching permeable surface with Cu/Al_2O_3 additives and unsteady two-dimensional Casson fluid flow over a stretching porous medium and employed with the shooting method for the numerical solution. It was observed that both the flow and heat transfer characteristics are altered for different values of the governing parameters such as unsteadiness parameter, Casson parameter, and Prandtl number. Mate *et al.* (2023) [18] investigated the thermal radiation effect on non-Newtonian Casson Fluid through a Porous Material over a magnetic field with buoyancy.

The suitable similarity transformation variables were employed to reduce the governing equations to non-linear ordinary differential equation. The Chebychev Collocation Method with the aid of Wolfram Mathematical software were employed to solve the resulting non-dimensional couple equations numerically. The study shows that velocity enhances as thermal and mass Grashof number is increase.

Ali *et al*. (2023) highlighted the mixed convective flow of hybrid nanofluid over a heated stretching disk with zero-mass flux using the modified Buongiorno model. The mathematical analysis of Casson fluid flow with energy and mass transfer under the influence of activation energy from a non-coaxially spinning disc were reviewed. A nonlinear sequence of partial differential equations was used to describe the phenomenon. The modeled equations were reduced to a non-dimensional set of ordinary differential equations (ODEs) using similarity replacement. The obtained sets of ODEs were further simulated using the parametric continuation method (PCM). The impact of physical constraints on energy, concentration, and velocity profiles are presented through figures and tables. It should be noted that the effect of the Casson fluid coefficient, the Grashof number, and the magnetic field reduces the fluid's primary velocity contour. The mass transfer field decreases with the action of constructive chemical reactions, but is augmented by the effects of destructive chemical reactions. The accelerating trend in Schmidt number lowers the mass profile, while it is enhanced by increasing values of activation energy and Soret number.

Hemmat *et al.* (2019) [13] studied Experimental investigation of effective parameters on MWCNT–TiO 2/SAE50 hybrid nanofluid viscosity and MHD effects on heat transfer over stretching sheet embedded in porous medium with variable viscosity, viscous dissipation and heat source/sink. The symmetry groups admitted by the corresponding boundary value problem are obtained by using Lie's scaling group of transformations. Similarity variables where used to reduce partial differential equations of the governing equations into self-similar non-linear ordinary differential equations. Numerical solutions of these equations are obtained by Runge-Kutta fourth order with shooting method. It was observed that the velocity profiles decrease with the increase in permeability parameter while temperature profiles increases with the increase in permeability parameter.

Jamshed *et al.* (2021) [15] studied the Casson nanofluid and examined the results for entropy and heat transport under solar thermal radiations. Sajid *et al.* (2023) [21] studied the second law for a parabolic trough surface collector (PTSC) located inside solar aircraft wings, by taking the homo/heterogeneous reaction. Kashi *et al*. (2020) formulated the model for $Cu\text{-}Al_2O_3$/water hybrid nanofluid using the single-phase technique and reported a detailed analysis. Recent investigations were revealed in the studies by Adnan *et al*. (2022a), Adnan *et al*. (2022b), Adnan *et al*., (2020), Adnan *et al*., (2022c), Adnan *et al*., (2022d), and Ahmed *et al*. (2017) [9].

2. Problem development

2.1 Problem statement and geometry

Considering steady 2-dimensional, non- Newtonian Casson hybrid nanofluid flow through a stretching surface embedded in Darcy-Forchiemer porous medium. The Riga plate with current density j_0, magnetization M_0 is place at boundary layer along horizontal direction to provide modified magnetic field. The space consists of highly permeable stretching porous medium packed with Casson hybrid nanofluid consists of Magnetite,Fe3O4 and Silver, Ag dissolves in Ethylene Glycol, ($C_2H_6O_2$) as a base fluid. The modified magnetic field supply the Lorentz force which control the fluid flow along the surface by reducing the hybrid nanofluid friction and pressure. The Riga plate also aids the delay of boundary layer separation and the reduction of turbulence impacts. The hybrid nanofluid fluid velocity components along (x, y) directions are denoted by (u, v) respectively, where y axis is orthogonal to the surface and$x$ - axis is along the stretching porous medium, and the stretching velocity is represented by $u_w(x)$ >0.

The schematic diagram of the flow geometry is show in Fig 1.

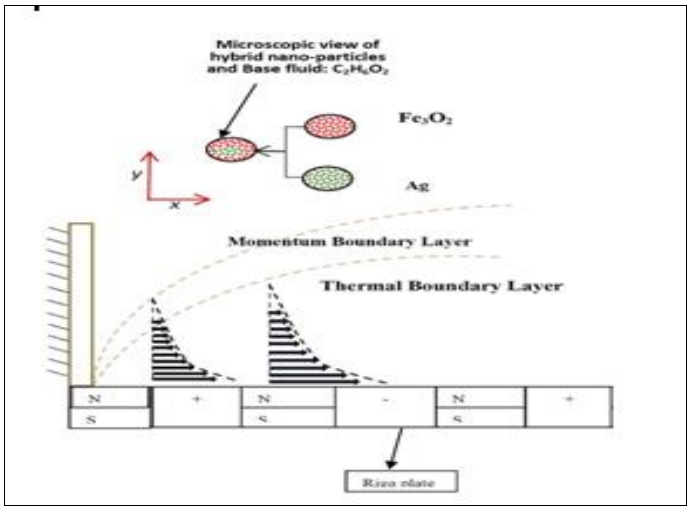

Fig 1.1: The flow geometry

$$\frac{\partial u}{\partial x}+\frac{\partial v}{\partial y}=0 \tag{1}$$

$$u\frac{\partial u}{\partial x}+v\frac{\partial u}{\partial y}=\frac{1}{\rho_{hnf}}\left(1+\frac{1}{\beta}\right)\frac{\partial}{\partial y}\left[\mu_{hnf}(T)\frac{\partial u}{\partial y}\right]+\frac{\pi j_0 M}{8\rho_{hnf}}e^{-\frac{\pi y}{s}}-\frac{\mu_{hnf}(T)}{\rho_{hnf}(kp)_0}\left(1-\frac{1}{\beta}\right)u-\frac{b^*}{(kp)_0}u^2 \tag{2}$$

$$u\frac{\partial T}{\partial x}+v\frac{\partial T}{\partial y}=\frac{1}{(\rho c_p)_{knf}}\frac{\partial}{\partial y}\left[K_{hnf}(T)\frac{\partial T}{\partial y}\right]+\frac{Q_0}{(\rho c_p)_{knf}}(T-T_\infty)+\left(1+\frac{1}{\beta}\right)\frac{\mu_{knf}(T)}{(\rho c_p)_{knf}}\left(\frac{\partial u}{\partial y}\right)^2-\frac{1}{(\rho c_p)_{knf}}\frac{\partial q_r}{\partial y}+\frac{b^*}{(\rho c_p)_{knf}(kp)_0}u^2+\frac{b^*}{(\rho c_p)_{knf}(kp)_0} \tag{3}$$

The proposed boundary conditions for this problem are defined as (Mate *et al*. 2024)

$$\left.\begin{array}{l} u=u_w, v=v_w, T=T_w, aty=0, \\ u\to 0=, T\to T_\infty, asy\to\infty \end{array}\right\} \tag{4}$$

The quantities appearing in the aforementioned governing laws are $\frac{\partial q_r}{\partial y}$ (radiative heat flux), V_{hnf} (Kinematic viscosity), ρhnf (Density), k_{hnf} (Thermal conductivity), (ρc_p) (specific heat capacity at constant pressure of the hybrid nanofluid), M (magnetization of the electrode, J_O (current), α_{hnf} (Thermal diffusivity), and B_O (Uniform magnetic field. The generalized form of above models and other thermophysical properties for ordinary nanofluid and hybrid nanofluid are provided through Table 1.

Table 1: Thermo-Physical properties comparison between nanofluid and hybrid nanofluid

These are the thermophysical characteristics of THNF:

Viscosity:

$$\mu_{(trihnf)}=\mu_f\left(1-\phi_{\mathrm{Ag}}\right)^{-2.5}\left(1-\phi_{\mathrm{Fe3O4}}\right)^{-2.5}\left(1-\phi_{\mathrm{Ag}}\right)^{-2.5},$$

Density:

$$\rho_{(trihnf)}=\rho_f\left\{\left(1-\phi_{\mathrm{Ag}}\right)\left[\left(1-\phi_{\mathrm{Fe3O4}}\right)\left(1-\phi_{\mathrm{Ag}}\right)+\phi_{\mathrm{Ag}}\frac{\rho_{\mathrm{Ag}}}{\rho_f}+\phi_{\mathrm{Fe3O4}}\frac{\rho_{\mathrm{TiO_2}}}{\rho_f}\right]+\phi_{\mathrm{Ag}}\frac{\rho_{\mathrm{Ag}}}{\rho_f}\right\},$$

Heat Capacity:

$$\left(\rho C_\rho\right)_{(trihnf)}=\left(\rho c_p\right)_f\left\{\left(1-\phi_{\mathrm{Ag}}\right)\left[\begin{array}{c}\left(1-\phi_{\mathrm{Fe3O4}}\right)\left(1-\phi_{\mathrm{Ag}}\right)+\phi_{\mathrm{Ag}}\frac{(\rho c_p)_{\mathrm{Ag}}}{(\rho c_p)_f}+\\ \phi_{\mathrm{Fe3O4}}\frac{(\rho c_p)_{\mathrm{Fe3O4}}}{(\rho c_p)_f}\\ +\phi_{\mathrm{Ag}}\frac{(\rho c_p)_{\mathrm{Ag}}}{(\rho c_p)_f}\end{array}\right]\right\}, \tag{5}$$

Electrical Conductivity:

$$\frac{\sigma_{(trihnf)}}{\sigma_{(dihnf)}} = \left(\frac{(1+2\phi_{Ag})\sigma_{Ag}+(1-2\phi_{Ag})\sigma_{(dihnf)}}{(1-\phi_{Ag})\sigma_{Ag}+(1+\phi_{Ag})\sigma_{(dihnf)}}\right), \frac{\sigma_{(dihnf)}}{\sigma_{nf}} = \left(\frac{(1+2\phi_{Fe3O4})\sigma_{Fe3O4}+(1-2\phi_{Fe3O4})\sigma_{nf}}{(1-\phi_{Fe3O4})\sigma_{Fe3O4}+(1+\phi_{Fe3O4})\sigma_{nf}}\right),$$

$$\frac{\sigma_{nf}}{\sigma_f} = \left(\frac{(1+2\phi_{Ag})\sigma_{Ag}+(1-2\phi_{Ag})\sigma_f}{(1-\phi_{Ag})\sigma_{Ag}+(1+\phi_{Ag})\sigma_f}\right),$$

Thermal Conductivity:

$$\frac{k_{(trihnf)}}{k_{(dihnf)}} = \left(\frac{k_{Ag}+2k_{(dihnf)}-2\phi_{Ag}(k_{(dihnf)}-k_{Ag})}{k_{Ag}+2k_{(dihnf)}+\phi_{Ag}(k_{(dihnf)}-k_{Ag})}\right), \frac{k_{(dihnf)}}{K_{nf}} = \left(\frac{k_{Fe3O4}+2k_{nf}-2\phi_{Fe3O4}(k_{nf}-k_{Fe3O4})}{k_{Fe3O4}+2k_{nf}+\phi_{Fe3O4}(k_{nf}-k_{Fe3O4})}\right),$$

$$\frac{K_{nf}}{K_f} = \left(\frac{k_{Ag}+2k_f-2\phi_{Ag}(k_f-k_{Ag})}{k_{Ag}+2k_f+\phi_{Ag}(k_f-k_{AgS})}\right).$$

Here subscripts f stands for fluid, bf for base fluid. Numerical values of thermophysical properties of base fluid (water) and nanoparticles (Iron oxide and copper) are provided in Table 2.

Table2: Thermo- physical properties of hybrid base fluid and nanoparticles

Physical properties	$C_2H_6O_2$	Ag	Fe_3O_4
$\rho\left(\frac{kg}{m^3}\right)$	1113.5	4970	4970
$C_p\left(\frac{J}{kg\cdot k}\right)$	2430	385	700
$k\left(\frac{W}{m\cdot k}\right)$	0.253	401.0	3.7

Similarity rules

The following similarity equations are designated to perform the dimensional analysis of the model:

$$\eta = y\sqrt{\frac{u_w}{v_f}}, \psi = \sqrt{v_f u_w}xf(\eta), \theta(\eta) = \frac{T-T_\infty}{T_m-T_\infty}, u = \frac{\partial\psi}{\partial y}, v = -\frac{\partial\psi}{\partial x} \tag{6}$$

The variable dynamic viscosity and thermal conductivity given as:

$$\left.\begin{aligned}\mu_{hnf}(T) &= \mu_{hnf}(1+\varepsilon_2-\varepsilon_2\theta)\\ K_{hnf}(T) &= K_{hnf}(1+\varepsilon_4-\varepsilon_4\theta)\\ \frac{1}{\sigma'} &= \frac{1}{\sigma}\left(1+\varepsilon'(T-T_\infty)\right), \varepsilon = \varepsilon'(T-T_\infty)\end{aligned}\right\} \tag{7}$$

Incorporating the similarity transformation in (6) and (7), equation (1) is identically satisfied.
Also, after using the above-defined transformations, the momentum and energy equations transformed into following form:

$$\left(1+\frac{1}{B}\right)[(1+\varepsilon_2-\varepsilon_{2\theta})f^{111}-\varepsilon_2 f^{11}\theta^1] - \varphi_A\varphi_B f^{1^2} + \varphi_A\varphi_B f f^{11} + \varphi^A\varphi_C Z e^{-B\eta} +$$

$$\rho_p\left(1+\frac{1}{B}\right)(1+\varepsilon_2-\varepsilon_2\theta)f^1 - \varphi_A\varphi_B F_s f^{1^2} = 0 \tag{8}$$

$$\theta^{11}+\varepsilon_4\theta\theta^{11}+\varepsilon_4\theta^{1^2}+\frac{\varphi_E p_r f\theta^1}{\varphi_D}+\frac{\varphi_E\delta\theta}{\varphi_D}+P_r E_c\left(1+\frac{1}{B}\right)\frac{(1+\varepsilon_2-\varepsilon_2\theta)}{\varphi_A\varphi_D}+\frac{3}{4}\frac{Nd\theta^{11}}{\varphi_D}+\frac{P_r\rho_p}{\varphi_E}pEc f^{'2}+\frac{1}{\varphi_E}Pr F sEc f^{'3} = 0 \tag{9}$$

The derivative with regard to η is denoted by the prime that goes with each profile and the boundary condition (4) becomes:

$$f(0) = s, f^1(0) = \xi + \left(1+\frac{1}{\beta}\right), \theta(0) = 1, \varphi(0) = 1$$

$$f^1(\infty)\to 0, \theta(\infty)\to 0, \varphi(\infty)\to 0 \tag{10}$$

$$k_{hnf} = k_f * \frac{k_{s1}+(m-1)k_f-(m-1)\phi_1(k_f-k_{s1})}{k_{s1}+(m-1)k_f+\phi_2(k_f-k_{s1})} *$$

$$\left(\frac{k_{s2}+k_f\,(m\text{-}1)\left(\frac{k_{s1}+(m-1)k_f-(m-1)\phi_1\left(k_f-k_{s1}\right)}{k_{s1}+(m-1)k_f+\phi_1\left(k_f-k_{s1}\right)}-(m\text{-}1)\varphi_2\left(k_f\left(\frac{k_{s1}+(m-1)k_f-(m-1)\phi_1\left(k_f-k_{s1}\right)}{k_{s1}+(m-1)k_f+\phi_1\left(k_f-k_{s1}\right)}\right)-k_{s2}\right)\right)}{k_{s2}+(m\text{-}1)k_f\left(\frac{k_{s1}+(m-1)k_f-(m-1)\phi_1\left(k_f-k_{s1}\right)}{k_{s1}+(m-1)k_f+\phi_1\left(k_f-k_{s1}\right)}\right)+\phi_2\left(k_f\left(\frac{k_{s1}+(m-1)k_f-(m-1)\phi_1\left(k_f-k_{s1}\right)}{k_{s1}+(m-1)k_f+\phi_1\left(k_f-k_{s1}\right)}\right)-k_{s2}\right)}\right) \quad (11)$$

The following are dimensionless parameter from the equations:

$\delta = \frac{Q_0}{(\rho c_p)_f u_w}$ is the heat source parameter, $Pr = \frac{c_p \mu_f}{K_f}$ is the Prandtl number, $Ec = \frac{u_w{}^2 x^2}{c_p(T_w - T_\infty)}$ is the Eckert number, $Nr = \left(\frac{4T^3{}_\infty \sigma^*}{k^* K_f}\right)$ is the radiation parameter, $Pp = \frac{b^*}{\rho_f (kp)_0}$ is the Porosity parameter, $Fs = \frac{b^*}{\varphi_e (\rho c_p)_f (kp)_0} u_w^{23}$ is Foichermer number. (12)

Numerical Solution

The MHD chemically reactive of Casson non-Newtonian nanofluid flow equations, the Chebyshev collocation scheme was used to make an approximation solution. The basic functions used in the process of solving the governing ODEs are described as a Chebyshev polynomial. The following components make up this technique: Assuming that the coefficients of the functions that depend on the Chebyshev collocation scheme solutions in the differential equations are unknown, the predicted results are substituted into the expressions that govern the scheme in order to generate residuals or errors. The assumed results are substituted into the expressions that control the scheme in order to generate residual errors. Subsequently, the scheme of collocation is utilized in order to minimize the residual errors. An algebraic expression must be generated and then computed in order to find the unknown coefficient values. The accuracy of the expression was improved by making a mapping for shifted Chebyshev from [0, 1] to [0, ∞] [35 and 36]. CCM is used here to numerically solve the boundary value problem in (8) – (10), where the following assumptions are made about the solutions for unknown functions $f(\eta)$ and $\theta(\eta)$ for the sum of the Chebyshev base function:

$$f(\eta) = \sum_{i=0}^{N} a_i T_i \left(\frac{2\eta}{L} - 1\right) \quad (13)$$

$$\theta(\eta) = \sum_{i=0}^{N} b_i T_i \left(\frac{2\eta}{L} - 1\right) \quad (14)$$

Where a_i and b_i are unknown constant coefficients to be determined. $T_i \left(\frac{2\eta}{L} - 1\right)$ is the shifted Chebyshev base function from $[-1,1]$ to $[0, L]$ where L stands for the edge of the boundary layer. In order to compute the values of unknown coefficients. The results obtained were presented graphically and discussed

To calculate the values of undetermined coefficients, equations (13) and (14) are substituted into (8) and (9) and becomes then

$$\left(1 + \frac{1}{B}\right)\left[(1 + \varepsilon_2 - \varepsilon_{2\theta}) f_\eta{}^3 - \varepsilon_2 f_\eta{}^2 \theta_\eta\right] - \varphi_A \varphi_B f_\eta{}^2 + \varphi_A \varphi_B f f_\eta{}^2 + \varphi^A \varphi_C Z e^{-B\eta}$$

$$\rho_p \left(1 + \frac{1}{B}\right)(1 + \varepsilon_2 - \varepsilon_2 \theta) f_\eta - \varphi_A \varphi_B F_s f_\eta{}^2 = 0 \quad (15)$$

For j = 1,2,Λ, N-1

$$\theta_\eta{}^2 + \varepsilon_4 \theta \theta_\eta{}^2 + \varepsilon_4 \theta_\eta{}^2 + \frac{\varphi_E p_r f \theta_\eta}{\varphi_D} + \frac{\varphi_E \delta \theta}{\varphi_D} + P_r E_c \left(1 + \frac{1}{B}\right)\frac{(1 + \varepsilon_2 - \varepsilon_2 \theta)}{\varphi_A \varphi_D} + \frac{3}{4}\frac{N d \theta_\eta{}^2}{\varphi_D} + \frac{P_r \rho_p}{\varphi_E} p E c f_\eta{}^2 + \frac{1}{\varphi_E} Pr\, F\, s E c f_\eta{}^3 = 0 \quad (16)$$

For j = 1,2,Λ, N-1

While the boundary conditions becomes.

$$f(0) = s, f_\eta(0) = \xi + \left(1 + \frac{1}{\beta}\right), \theta(0) = 1, \varphi(0) = 1$$

$$f^1(\infty) \to 0, \theta(\infty) \to 0, \varphi(\infty) \to 0 \quad (17)$$

The residues $R_f(\eta, a, b)$ and $R_f(\eta, a, b)$ are obtained by plugging into equation (15), (16) and (17). Using the collocation approach, the residues are reduced to the smallest.

For $\delta(\eta - \eta_k) = \begin{cases} 1.\eta = \eta_k \\ 0.otherwise \end{cases}$

$$\int_0^L R_f \delta(\eta - \eta_k) d\eta = R_f(\eta_j) = 0, \quad (18)$$

For j = 1,2,Λ, N-1

$$\int_0^L R_f \delta(\eta - \eta_k) d\eta = R_\theta(\eta_j) = 0, \quad (19)$$

For j = 1,2,Λ, N-1

Where $\eta_j = \frac{L}{2}\left[1 - cos\left(\frac{j\pi}{N}\right)\right]$ is the shifted Gauss-Lobatto point.

In this manner, equations (15) to (19) form a system of 3N+3 algebraic equations with3N+3 unknown constant coefficients, a_i and b_i. The resulting algebraic equations were solved, and the values of constant coefficients are found using the MATHEMATICA version 11.3 program. The value of L is set to 12 to ensure that all numerical solutions accurately respect the far- field asymptotic

Results and discussion against the physical constraints

The physical flow constraints are imperative to analyze the fluid motion and thermal behavior over a desired region. For the sake of this purpose, the results are organized to examine the hybrid nanofluid dynamics.

The velocity behavior of (Ag-Fe_3O_4)/ethylene glycol and Ag/ethylene glycol

Fig 2 demonstrates the velocity of [(Ag-Fe_3O_4)/ethylene glycol]$_{hnf}$ and [Ag/blood]$_{nf}$ against the imposed magnetic field (Fig 3) aligned vertically to the plane of flow. The results reveal that the velocity (F′(η) and G′(η)) of Ag-Fe_3O_4)/ethylene glycol]$_{hnf}$ and [Ag/ethylene glycol]$_{hnf}$ drops for the magnetic parameter effects M. Physically, the aligned magnetic field opposes the fluid motion due to which the fluid particles move slowly. In the surroundings of the surface, these effects are optimum and the motion gradually reduces far from the sheet and finally vanishes at an ambient location from the surface. Thus, the motions of [Ag-Fe_3O_4)/ethylene glycol]$_{hnf}$ and [Ag/ethylene glycol]$_{hnf}$ can be controlled by strengthening the aligned magnetic field which is a significant physical phenomena.

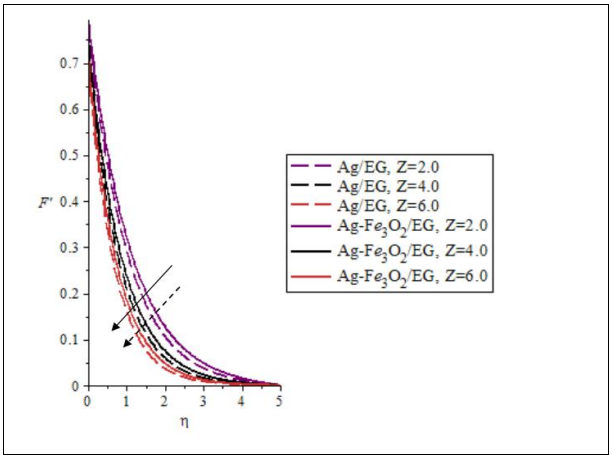

Fig 2: Effect of various values of Modified Magnetic term on fluid Velocity Profile

Fig 3 elaborate the effect of the variable viscosity parameter (ε_2) on velocity$F'(\eta)$. Viscosity is a measure of the fluid's resistance to flow. The higher the viscosity, the more resistance there is to the fluid's movement. This resistance causes a decrease in fluid velocity. This is because as viscosity increases, the fluid becomes more resistant to shear forces, which slow down the movement of the fluid

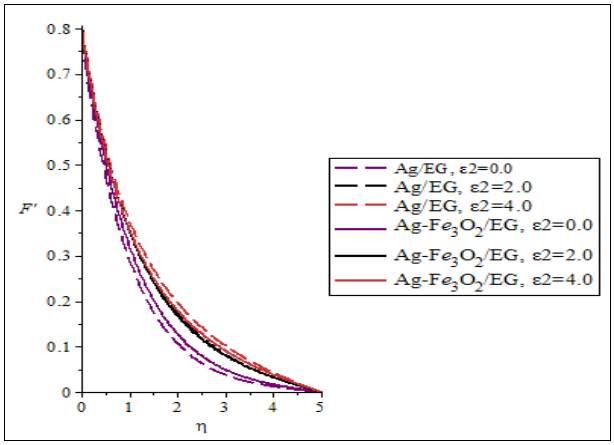

Fig 3: Effect of various values of variable viscosity on fluid Velocity F ' (η)

Fig 4 highlights the effects of Casson fluid parameter β on hybrid nanofluid velocity. The fluid velocity declines as the value of Casson fluid parameter is increasing. This is because increase in Casson parameter leads to the increase in strength of dynamic viscosity which consequently impede the flow along the stretching porous medium. This agrees with works of Kumar *et al.* (2016) [17], Waini *et al*. (2018), and Adeosun *et al.* (2021) [1].

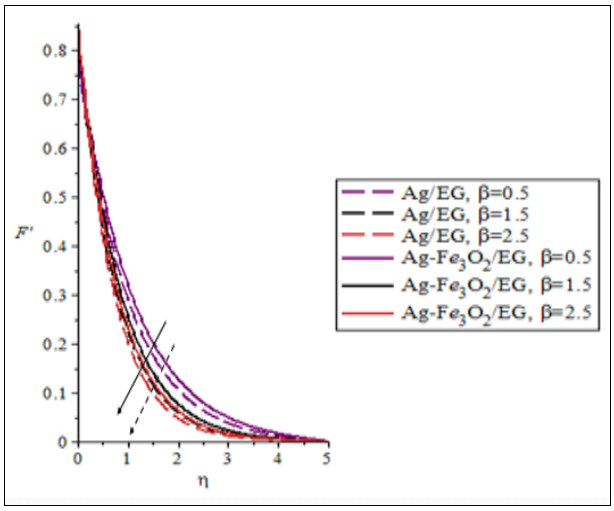

Fig 4: Effect of various values of Casson fluid β parameter on velocity F ' (η)

Fig 5 it is evident that rising values of porosity reduce the fluid flow in a stretching porous medium. This is because of an increase in porosity parameter associated with a reduction in flow permeability of which results in retardation of nanofluid flow. The fluid has more space to flow through the material, which reduces the amount of resistance to flow.

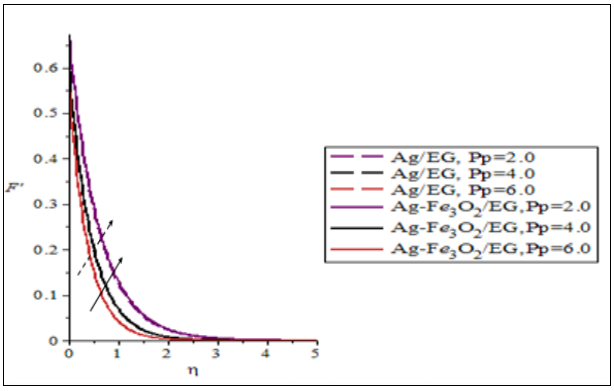

Fig 5: Effect of Various values of Porosity Parameter (Pp) on F ' (η)

Fig 6 explained the effects of Hartman number on the velocity of hybrid nanofluid. It is observed that as the value of (*Z*) rises, the velocity is elevated. This means that rising values of (*Z*) correspond to the higher intensity of the magnetic field strength mounted on the parallel plate which leads to the enhancement of the nanofluid flow over the plate by reducing the fluid friction. This validated the work of (Adeosun *et al*., 2021) [1].

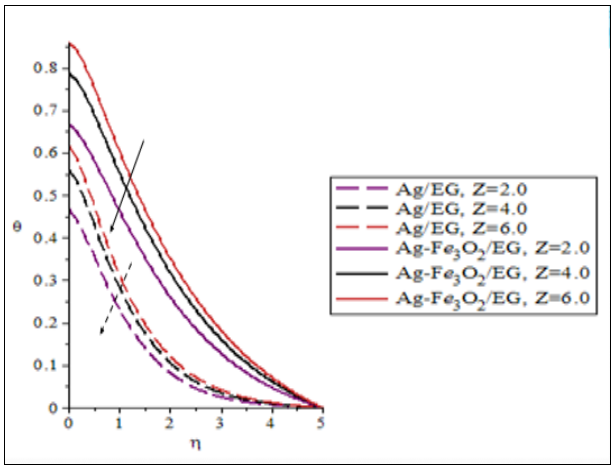

Fig 6: Effect of various values of Hartmann number on Temperature Profile

Fig 7 explained the effect of the Eckert number on the temperature profile. The Eckert number is a dimensionless number that defines the connection between the fluid kinetic energy and enthalpy. It expresses the change of kinetic energy into internal energy by the work done against the viscous fluid stress. The positive Eckert number illustrates the cooling of the medium, i.e. loss of heat to the fluid from the plate. It is clear that an increase in the Eckert number causes a decrease in the temperature profile.

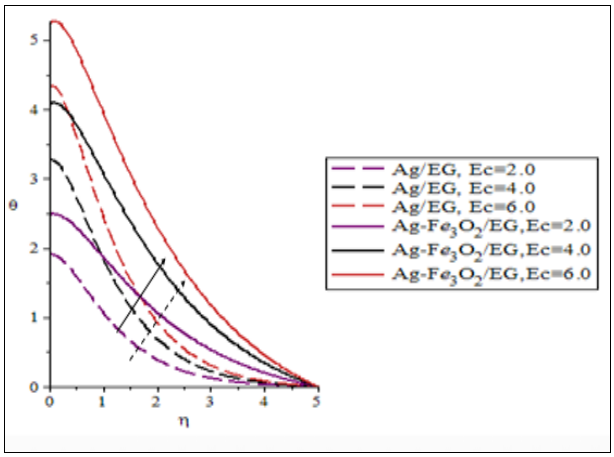

Fig 7: Effect various values of Eckert number Ec on temperature

Fig 8 explain the relationship between variable thermal conductivity (ε4) and temperature. The thermal conductivity of most materials increases with temperature because the molecules of a material move faster at higher temperatures, which allows them to transfer heat more efficiently.

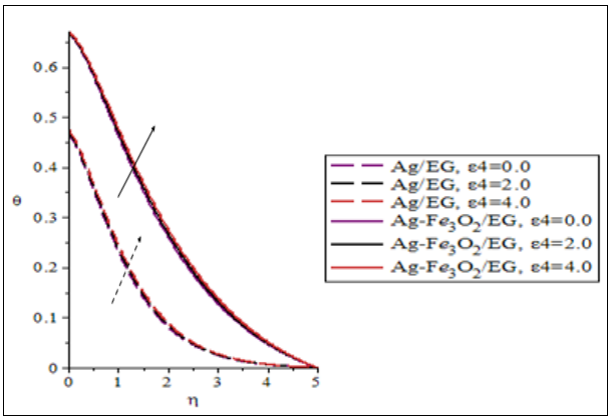

Fig 8: Effect various values of variable thermal conductivity term on temperature

Fig 9 shows that increase in thermal radiation parameter (Nd) enhance temperature of hybridnanofluid. Clearly it is evident that thermal radiation contributes in increasing temperature distribution because radiation enhances the internal energy of fluid and therefore, temperature rises. This validate the work of Ishtiaq *et al*, (2023) [14].

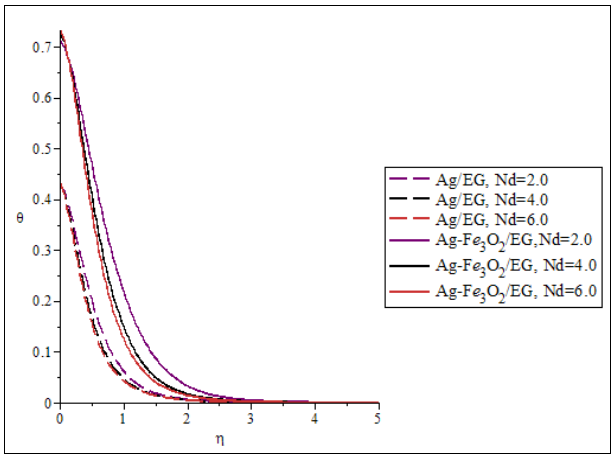

Fig 9: Effect various values Radiation Parameter Nd on temperature

Fig 10 explain the relationship between the Prandtl number and temperature. Prandtl number is an important parameter in the design of heat transfer and an increase in Prandtl number lead to a decrease in temperature because the thermal diffusivity of the fluid is lower thereby heat diffuses more slowly from the surface of the solid into the fluid.

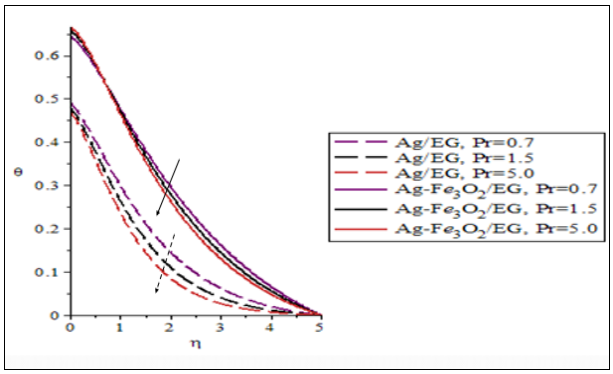

Fig 10: Effect of various values of prandtl number Pr on Temperature Profile

Conclusion

In this study, mathematical analysis of effect of variable properties of Fe_3O_4-Ag/EG Casson fluid flow through a porous medium with a modified magnetic field was investigated. The Casson fluid model was employed to capture the non-newtonian behavior of the fluid. The governing equations were transformed into dimentionless form using similarity variables and solved numerically using Chebychef Collocation method. The results demonstrated that

- The movement of $[(Ag\text{-}Fe_3O_4)/\text{ethylene glycol}]_{hnf}$ and $[Ag/EG]_{hnf}$ could be controlled against the high strength of the magnetic field which is beneficial for industrial applications.
- the magnetic field strength significantly influence the flow behavior.
- a stronger magnetic field leads to a reduction in velocity due to the Lorentz force.
- the Casson fluid parameter also plays a crucial role in regulating the flow characteristics.
- a higher Casson fluid parameter indicates a thicker yield stress, which reduces the velocity near the porous medium boundary.
- the porosity parameter, on the other hand, promotes fluid flow by providing additional pathways for the fluid to pass through.
- increasing the nanoparticles volume fraction enhanced the thermal conductivity of the fluid, leading to a more pronounced temperature distribution.

Data availability statement

The raw data supporting the conclusions of this article will be made available by the authors, without undue reservation. The data will be provided upon reasonable request.

Author contributions

All authors listed have made a substantial, direct, and intellectual contribution to the work and approved it for publication. Olusegun Adebisi wrote original draft, A. A. Bepo and M. Taiwo done mathematical analysis, and O. A. Ajala potentially contributed revision, language editing and study validation.

References

1. Adeosun AT, Gbadeyan JA, Lebelo RS. Heat Transport of Casson nanofluid flow over a melting Riga plate embedded in a porous medium. An International Journal of Engineering Research in Africa. 2021; 55:15-27.
2. Adnan, Ashraf W. Numerical Thermal Featuring in γAl_2O_3-$C_2H_6O_2$ Nanofluid under the Influence of Thermal Radiation and Convective Heat Condition by Inducing Novel Effects of Effective Prandtl Number Model (EPNM). Adv. Mech. Eng. 2022a; 14:168781322211065. Doi: 10.1177/16878132221106577
3. Adnan, Ashraf W. Thermal Efficiency in Hybrid (Al_2O_3-CuO/H_2O) and Ternary Hybrid Nanofluids (Al_2O_3-CuO-Cu/H_2O) by Considering the Novel Effects of Imposed Magnetic Field and Convective Heat Condition. Waves Random Complex Media, 2022b. Doi: 10.1080/17455030.2022.2092233
4. Adnan, Khan U, Ahmed N. Thermal Enhancement and Entropy Investigation in Dissipative ZnO-SAE50 under Thermal Radiation: a Computational Paradigm. Waves Random Complex Media, 2022. Doi: 10.1080/17455030.2022.2053243
5. Adnan SZA, Khan U, Abdeljawad T, Ahmed N, Khan I, Nisar KS, *et al*. Investigation of Thermal Transport in Multi-Shaped Cu Nanomaterial-Based Nanofluids. Materials. 2020; 13:2737. Doi: 10.3390/ma13122737
6. Adnan SZA, Zaidi U, Khan N, Ahmed Y, Chu M, Khan I, *et al*. Impacts of Freezing Temperature Based Thermal Conductivity on the Heat Transfer Gradient in Nanofluids: Applications for a Curved Riga Surface. Molecules. 2020; 25:2152. Doi:10.3390/molecules25092152
7. Adnan WA, Andualem M, Khan I. Thermal Transport Investigation and Shear Drag at Solid–Liquid Interface of Modified Permeable Radiative-SRID Subject to Darcy–Forchheimer Fluid Flow Composed by γ-nanomaterial. Sci. Rep. 2022; 12:3564. Doi: 10.1038/s41598-022-07045-2

8. Adnan Ashraf W, Alghtani AH, Khan I, Andualem M. Thermal Transport in Radiative Nanofluids by Considering the Influence of Convective Heat Condition. J. Nanomater, 2022, 1-11. Doi: 10.1155/2022/1854381
9. Ahmed N, Adnan, Khan U, Mohyud-Din ST. Influence of Thermal Radiation and Viscous Dissipation on Squeezed Flow of Water between Riga Plates Saturated with Carbon Nanotubes. Colloids Surfaces a Physicochem. Eng. Aspects. 2017; 522:389-398. Doi: 10.1016/j.colsurfa.2017.02.083
10. Ali B, Mishra NK, Rafique K, Jubair S, Mahmood Z, Eldin SM. Mixed convective flow of hybrid nanofluid over a heated stretching disk with zero-mass flux using the modified Buongiorno model. Alexandria Engineering Journal. 2023; 72:83-96.
11. Ali L, Liu X, Ali B, Abdal S, Zulqarnain RM. Finite element analysis of unsteady MHD Blasius and Sakiadis flow with radiation and thermal convection using Cattaneo-Christov heat flux model Phys. Scr. 2023; 96(12):article-125219. Doi: 10.1088/1402-4896/ac25a3
12. Awais M, Salahuddin T. Variable thermophysical properties of magnetohydrodynamic cross fluid model with effect of energy dissipation and chemical reaction Int. J. Mod. Phys. B. 2023; article-2450197. Doi: 10.1142/S0217979224501972
13. Hemmat Esfe M, Alidoust S, Mohammadnejad Ardeshiri E, Kamyab MH, Toghraie D. Experimental investigation of effective parameters on MWCNT–TiO 2/SAE50 hybrid nanofluid viscosity and MHD effects on heat transfer over stretching sheet embedded in porous medium with variable viscosity, viscous dissipation and heat source/sink. Nanoscale Research Letters. 2019; 17(1):4.
14. Ishtiaq B, Nadeem S, Alzabut J. Effects of variable magnetic field and partial slips on the dynamics of Sutterby nanofluid due to biaxially exponential and nonlinear stretchable sheets. Heliyon. 2023; 9(7).
15. Jamshed W, Devi SU, Nisar KS. Single phase-based study of Ag-Cu/EO Williamson hybrid nanofluid flow over a stretching surface with shape factor. Physica Scripta. 2021; 96(6):065202.
16. Khashi NS, Arifin NM, Pop I. Mixed Convective Stagnation Point Flow towards a Vertical Riga Plate in Hybrid Cu-Al_2O_3/Water Nanofluid. Mathematics. 2020; 8(6):912. Doi: 10.3390/math8060912
17. Kumar V, Pare A, Tiwari AK, Ghosh SK. Efficacy evaluation of oxide-MWCNT water hybrid nanofluids: An experimental and artificial neural network approach. Colloids and Surfaces A: Physicochemical and Engineering Aspects. 2016; 620:126562.
18. Mate SO, Obalalu AM, Ajala OA, Bakare TB, Ogunsola AW, Akindele AO. Thermal radiation effect on non-newtonian casson fluid flow through a porous material over a magnetic field with buoyancy, 2023.
19. Pattnaik PK, Mishra S, Baag S. Heat transfer analysis on Engine oil-based hybrid nanofluid past an exponentially stretching permeable surface with Cu/Al2O3 additives. Proceedings of the Institution of Mechanical Engineers, Part N: Journal of Nanomaterials, Nanoengineering and Nanosystems. 2023; 237(1-2):3-17.
20. Ramzan M, Alotaibi H. Variable viscosity effects on the flow of MHD hybrid nanofluid containing dust particles over a needle with Hall current: A Xue model exploration. Communications in Theoretical Physics. 2022; 74(5):055801.
21. Sajid T, Jamshed W, Eid MR, Altamirano GC, Aslam F, Alanzi AM, Abd-Elmonem A. Magnetized Cross tetra hybrid nanofluid passed a stenosed artery with nonuniform heat source (sink) and thermal radiation: Novel tetra hybrid Tiwari and Das nanofluid model. Journal of Magnetism and Magnetic Materials. 2023; 569:170443.
22. Salahuddin T, Awais M. Numerical computation of joule heating and chemical reaction for the radiated Casson fluid on the slender parabolic surface. ZAMM-Journal of Applied Mathematics and Mechanics/Zeitschrift für Angewandte Mathematik und Mechanik. 2024; 104(4):e202300647.
23. Xuan Z, Zhai Y, Li Y, Li Z, Wang H. Guideline for selecting appropriate mixing ratio of hybrid nanofluids in thermal management systems. Powder Technology. 2022; 403:117425.
24. Waini I, Ishak A, Pop I. Radiative and magnetohydrodynamic micropolar hybrid nanofluid flow over a shrinking sheet with Joule heating and viscous dissipation effects. Neural Computing and Applications. 2022; 34(5):3783-3794.
25. Zeeshan Ahammad NA, Shah NA, Chung JD. Role of Nanofluid and Hybrid Nanofluid for Enhancing Thermal Conductivity towards Exponentially Stretching Curve with Modified Fourier Law Inspired by Melting Heat Effect. Mathematics. 2023; 11(5):1170.